Carbohydrate Research, 238 (1993) 49–73
Elsevier Science Publishers B.V., Amsterdam

A Monte Carlo method for conformational analysis of saccharides

Thomas Peters [a], Bernd Meyer [b], Rainer Stuike-Prill [b], Ray Somorjai [c] and Jean-Robert Brisson [c]

[a] *Institute for Biophysical Chemistry, University of Frankfurt, Theodor-Stern-Kai 7-15, Building 75 A, D-6000 Frankfurt (Germany)*
[b] *Complex Carbohydrate Research Center and Department of Biochemistry, The University of Georgia, Athens, Georgia 30602 (USA)*
[c] *Institute for Biological Sciences, National Research Council of Canada, Ottawa, Ontario K1A OR6 (Canada)*

(Received March 3rd, 1992; accepted June 3rd, 1992)

ABSTRACT

A Metropolis Monte Carlo (MMC) algorithm was applied to explore conformational spaces spanned by the exocyclic dihedral angles of four disaccharides α-D-Man(1 → 3)-α-D-Man(1 → O)Me (**1**), α-D-Man(1 → 2)-α-D-Man(1 → O)Me (**2**), methyl β-cellobioside (**3**), and methyl β-maltoside (**4**). The simulation method uses the HSEA force field and randomly samples the conformational space with an automatic preference for low-energy states. In comparison to a systematic grid search, MMC offers a much more convenient and efficient protocol for the computation of ensemble average values of experimentally accessible NMR parameters such as NOE effects or ^3J coupling constants. Energy barriers of a few kcal/mol were found to be surmounted easily when running the simulations with the temperature parameter set at room temperature, whereas passing significantly higher barriers required elevated temperature parameters. Ensemble average NOE values were calculated using the MMC technique and a conventional systematic grid search showing that the MMC method adequately samples the conformational spaces of **1**–**4**. Theoretical NOEs derived for global or local minimum conformations are different from ensemble average values, and it is shown that averaged NOEs agree significantly better with experimental data. Ensemble average NOEs for **1** derived from MMC/HSEA, and previously reported MM2CARB and AMBER calculations all showed good agreement with experimental data, with MMC/HSEA giving the closest fit.

INTRODUCTION

An important goal of conformational analysis of oligosaccharides is to establish a link between their three-dimensional structure and specific biological activity[1,2].

Correspondence to: Dr. T. Peters, Institute for Biophysical Chemistry, University of Frankfurt, Theodor-Stern-Kai 7-15, Building 75 A, D-6000 Frankfurt, Germany; *or to*: Dr. J.-R. Brisson, Institute for Biological Sciences, National Research Council of Canada, Ottawa, Ontario, Canada K1A OR6.

The most frequently used tools for investigating the solution conformation of carbohydrate chains have been NOE experiments in conjunction with empirical force-field calculations[3,4]. Whereas, such experiments have been very successfully applied to determine the preferred solution conformation of proteins[5], usually only a limited number of interglycosidic NOEs are available for saccharides, and thus unambiguous assignment of a three dimensional oligosaccharide structure in aqueous solution solely based upon NOE restraints is impossible in most cases[6]. Attempts to surmount this problem involved the determination of additional NMR experimental restraints such as special deshielding effects[7], vicinal homo- and hetero-nuclear coupling constants[8], and chemical shifts of anomeric carbon atoms[9]. Recently, it has been shown that certain NMR pulse sequences allow the detection of dipolar contacts between hydroxyl group protons and remote ring protons in water, thus furnishing additional conformational restraints[10]. Still, the problem remains that, in general, carbohydrate chains exhibit significantly more conformational flexibility than found in globular proteins, and the application of NOE restraints alone may well indicate high-energy conformations[6] rather than true minima. Therefore, statistical mechanics calculations on the basis of energy surfaces derived from force-field calculations have been performed employing a systematic grid search (GS) to yield ensemble average values of NMR parameters such as NOEs, spin–lattice relaxation times (T_1), and vicinal coupling constants. The theoretical parameters obtained in this fashion were then compared to experimentally derived values, and the results available so far indicate that this averaging procedure improves the fit between experimental and theoretical NMR data[6,11–14]. In order to cover the complete conformational space for a more complex oligosaccharide by a systematic GS, calculations have to be performed for a large number of conformers. Consequently, extension of this method towards larger saccharides or more sophisticated force-fields requires a decrease of conformational space and thus knowledge about its low-energy parts. The same type of problem is well known, in the field of statistical physics, to occur with the simulation of any property of a multi-particle system[15] and is of crucial importance for the simulation of liquids[16]. In these areas, Monte Carlo algorithms[17] have been widely used to calculate average thermodynamic properties. Monte Carlo simulations were also successfully used in attempts to surmount the multiple-minima problem in protein folding[18–20].

A few studies utilizing Monte Carlo methods for the conformational analysis of oligosaccharides have been published. These investigations have been concerned with the exploration of preferred conformations of glycopeptides[21], with the determination of average conformational energies of mono- and di-saccharides[22,23], and with the examination of configurational and conformational properties of amylose chains[24,25]. No attempts have been made thus far to derive ensemble average NMR parameters. We present a Metropolis Monte Carlo (MMC) method for the conformational analysis of oligosaccharides that is capable of giving the same results for averaged NMR parameters as the systematic GS approach just

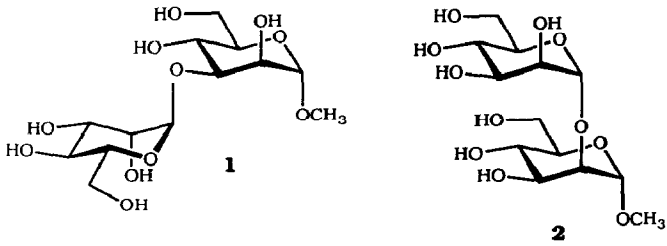

1

2

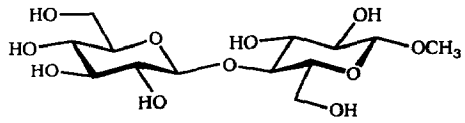

3

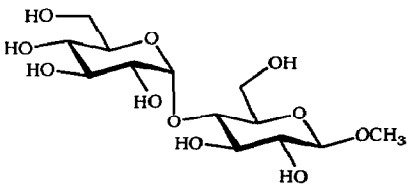

4

described, but offering a more convenient protocol. The hard sphere exo-anomeric (HSEA) force field[7] is chosen as the basis for the MMC simulations. Although there are known disadvantages of this simple type of force field, such as overly steep potential-energy wells, it has been successfully applied in the past to approximate experimental NOEs[6,13]. The method was applied to two α-linked mannose disaccharides, **1** with a (1 → 3) and **2** with a (1 → 2) linkage, and to the two ubiquitously occurring glucose disaccharides, cellobiose **3** with a β-(1 → 4) and maltose **4** with and α(1 → 4) linkage, respectively, as their methyl α-glycosides for **1** and **2**, and methyl β-glycosides for **3** and **4**. The results are compared to data stemming from statistical mechanics calculations utilizing the more conventional GS technique and to experimental NOE data.

EXPERIMENTAL

Computational methods.—Minimum-energy conformations and energy surfaces were calculated using the program GESA[26] that applies the HSEA force field. Dihedral angles ϕ and ψ at the glycosidic linkages, and ω at the C-5–C-6 bonds were defined as follows: ϕ = H-1–C-1–O-1–C-X, ψ = C-1–O-1–C-X–H-X, with X being the aglyconic linkage site, and ω = O-6–C-6–C-5–O-5. The three staggered

rotamers were denoted as *gg* ($\omega = -60°$), *gt* ($\omega = 60°$), and *tg* ($\omega = 180°$) according to IUPAC nomenclature. Glycosidic bond angles were fixed at 117° and pyranose rings were treated as rigid units residing in the $^4C_1$ conformation. Coordinates were taken from neutron-diffraction data[27] with the hydrogen atoms deleted and placed at standard geometries. Treatment of hydroxyl protons was avoided deliberately and, consequently, hydrogen bonds were not taken into account. No extra torsional potential function was used to describe the rotation of the hydroxymethyl groups of the hexopyranose units.

Monte Carlo simulations were performed applying the MMC algorithm[28]. The MMC program uses the geometry of saccharides (GESA) routines to calculate molecular geometries and conformational energies. During these simulations, all exocyclic dihedral angles ϕ, ψ, and ω were treated as flexible, giving rise to conformational spaces with six dimensions for **1–4**. The MMC algorithm comprises several steps that are summarized in the following: (*1*) A low energy conformer is chosen as the initial conformation and its energy is calculated. (*2*) An MMC step is defined as the move of one single parameter. The dihedrals are altered in a regular fashion, one by one, until all angles to be varied have been moved. A complete sweep through all variable angles is called a macro step or macro move. The generation of new conformational states is achieved by adding random step lengths $\pm\Delta\phi$, $\pm\Delta\psi$, and $\pm\Delta\omega$ to the dihedral angles ϕ, ψ, ω, spanning the conformational space. A maximum step length has to be assigned to each direction in conformational space. (*3*) The energy difference $\Delta E = E_{new} - E_{old}$ between the newly generated conformation state (E_{new}) and the previous state (E_{old}) is usually calculated after each macro step. If ΔE is negative or zero, the move is always accepted, otherwise the Metropolis test[28] is applied. A random number ξ is generated in the interval [0,1] and compared to the Boltzmann factor $\exp(-\Delta E/RT)$, where R is the gas constant and T the temperature. If ξ is smaller than the Boltzmann factor, the move is accepted and the altered conformation is counted as the new state. If ξ is greater, the old conformation is kept and the old state is counted as a new state, thus ensuring that on average each conformational state is visited with a frequency according to its statistical weight. Alternatively, the Metropolis test may be performed after each single MMC step. Although this in general leads to a higher acceptance ratio for given step lengths, in most cases the method is much slower, movements may be strongly correlated[17], and convergence of running averages over the space will be reached only after a longer time[29]. Therefore, in this study, the Metropolis test is always performed after a macro move. (*4*) Steps *2* and *3* are repeated until convergence of running averages of a property A of interest (e.g., NOEs, distances, potential energy, etc.) is achieved. In the following text, repeated cycling through steps *2* and *3* without data collection will be referred to as "equilibration period". (*5*) As soon as running averages of A have converged, an equilibrium phase is reached and ensemble average values $\langle A \rangle$ may be determined from the simulation by simply calculating the arithmetic mean over an adequate number of macro moves:

TABLE I

Relative NOE values for 1. Values for average NOEs are calculated at 300 K. The values in parentheses give the corresponding results at 600 K

Proton satd	Proton obsd	Experiment [a]	Global minimum [b]	$\langle NOE \rangle_{GS}$ $(\langle r^{-6} \rangle)$	$\langle NOE \rangle_{GS}$ $(\langle r^{-3} \rangle^2)$	$\langle NOE \rangle_{MMC}$ $(\langle r^{-6} \rangle)$	$\langle NOE \rangle_{MMC}$ $(\langle r^{-3} \rangle^2)$	$\langle NOE \rangle_{GS}$ MM2CARB [c]	$\langle NOE \rangle_{MD}$ AMBER [d]
H-1′	H-2′	1.00	1.00	1.00	1.00	1.00 (1.00)	1.00 (1.00)	1.00	1.00
	H-2	0.00	−0.05	−0.01	−0.03	−0.01 (0.07)	−0.04 (0.00)	0.30	0.04
	H-3	1.00	0.84	1.00	0.98	0.97 (1.00)	0.95 (0.98)	0.90	0.86
	H-4	0.08	0.09	0.07	0.06	0.05 (0.05)	0.05 (0.05)	0.02	n.d. [f]
H-2	H-1	1.00	1.00	1.00	1.00	1.00 (1.00)	1.00 (1.00)	1.00	1.00
	H-3	0.90	0.69	0.63	0.65	0.80 (0.81)	0.69 (0.69)	n.d.	n.d.
	H-5′	0.60	0.76	0.65	0.60	0.92 (0.82)	0.73 (0.58)	0.80	0.96
SD [e]			0.12	0.10	0.10	0.09 (0.09)	0.10 (0.08)	0.15	0.17

[a] Ref. 31; [b] $\phi = -49°$, $\psi = -10°$; [c] Ref. 12; [d] Ref. 43; [e] See Computational methods. [f] Not determined.

TABLE II

Relative NOE values for **2**. Values for average NOEs are calculated at 300 K. The values in parentheses give the corresponding results at 600 K

Proton satd	Proton obsd	Experiment [a]	Global minimum [a]	$\langle NOE\rangle_{GS}$ $(\langle r^{-6}\rangle)^a$	$\langle NOE\rangle_{GS}$ $(\langle r^{-3}\rangle^2)^a$	$\langle NOE\rangle_{MMC}$ $(\langle r^{-6}\rangle)$	$\langle NOE\rangle_{MMC}$ $(\langle r^{-3}\rangle^2)$
H-1′	H-2′	1.00	1.00	1.00	1.00	1.00 (1.00)	1.00 (1.00)
	H-2	1.38	0.82	1.04	1.00	1.04 (1.08)	1.01 (1.07)
H-2′	H-1′	1.00	1.00	1.00	1.00	1.00 (1.00)	1.00 (1.00)
	H-3′	1.44	1.33	1.50	1.50	1.54 (1.69)	1.48 (1.58)
H-1	H-2	1.00	1.00	1.00	1.00	1.00 (1.00)	1.00 (1.00)
	H-5′	1.04	1.38	1.50	1.38	1.67 (1.61)	1.57 (1.34)
H-2	H-3	1.00	1.00	1.00	1.00	1.00 (1.00)	1.00 (1.00)
	H-1′	1.79	1.05	1.21	1.19	1.21 (1.21)	1.19 (1.20)
SD			0.35	0.29	0.28	0.32 (0.32)	0.31 (0.26)

[a] Ref. 14; the global minimum conformation is: $\phi = -49°$, $\psi = -19°$ with the hydroxymethyl groups fixed in the *gg* conformation.

$\langle A\rangle = \Sigma_i A_i/M$, where A is the observable parameter, M the total number of MMC macro moves, and i is the conformational state. The ensemble of conformational states of the equilibrium phase should approach, in the limit, thermodynamic equilibrium. Average values from MMC calculations are marked with a subscript "MMC" to distinguish them from average values derived via systematic grid searches, labelled with the subscript "GS" (cf. Tables I–IV).

MMC simulations for **1–4** were performed at 300 and 600 K with 250 000 macro steps each. Conformational states > 1000 kcal/mol higher in energy than the previous state were rejected without calculating the Boltzmann factor in order to avoid underflow errors during exponentiation. The total acceptance ratio (total number of accepted moves/total number of moves) as well as the local acceptance ratio (number of accepted moves/last n moves) were calculated every $n = 100$ macro steps during an equilibration period of 2000 macro moves, and every $n = 1000$ macro steps during data accumulation. The local acceptance ratio was adjusted to a value between 0.2 and 0.5 performing test runs of 1000 to 5000 macro moves with different maximum step lengths. Maximum step lengths of 20° were found to give satisfactory acceptance ratios for **1–4**. At a given step length, the acceptance ratio is a measure for the shape of the particular minimum the system is residing in. It is obvious that sudden changes of the local potential-energy surface characteristics are much better reflected following the local acceptance ratio, instead of the overall acceptance ratio. In all cases, the equilibration period was monitored by calculating $\langle r^{-6}\rangle_{MMC}$ values corresponding to proton–proton distances r across the glycosidic linkage as a function of the number of macro moves. These values served as an estimate for the corresponding interglycosidic NOE. The interglycosidic proton pairs, selected for this monitoring process, were known to be sensitive towards glycosidic linkage conformation, which was easily

TABLE III

Relative NOE values for **3**. Values for average NOEs are calculated at 300 K. The values in parentheses give the corresponding results at 600 K.

Proton satd	Proton obsd	Experiment [a]	Minima [b]				$\langle NOE\rangle_{GS}$ $(\langle r^{-6}\rangle)$	$\langle NOe\rangle_{GS}$ $(\langle r^{-3}\rangle^2)$	$\langle NOE\rangle_{MMC}$ $(\langle r^{-6}\rangle)$	$\langle NOE\rangle_{MMC}$ $(\langle r^{-3}\rangle^2)$
			A	B	C	D				
H-1′	H-2′	n.d. [c]								
	H-3′ and H-5′	1.00	1.00	1.00	1.00	1.00	1.00	1.00	1.00 (1.00)	1.00 (1.00)
	H-4	0.59	0.72	0.02	0.08	−0.02	0.76	0.75	0.60 (0.63)	0.62 (0.64)
	H-3, H-6a, H-6b	0.28	0.09	0.05	1.30	1.57	0.09	0.09	0.12 (0.12)	0.09 (0.07)
	H5	0.13	−0.01	0.01	−0.05	0.80	−0.01	−0.01	−0.01 (−0.01)	0.00 (−0.01)
SD			0.13	0.31	0.58	0.79	0.14	0.14	0.10 (0.11)	0.12 (0.13)

[a] Ref. 45; [b] Minimum A: $\phi = 57°$, $\psi = -2°$, $E_{rel} = 0.00$ kcal/mol. Minimum B: $\phi = 168°$, $\psi = 0°$, $R_{rel} = 2.95$ kcal/mol. Minimum C: $\phi = 59°$, $\psi = -146°$, $E_{rel} = 6.99$ kcal/mol. Minimum D: $\phi = 28°$, $\psi = 173°$, $E_{rel} = 8.53$ kcal/mol; hydroxymethyl groups are fixed in the *gg* conformation. [c] Not determined.

TABLE IV

Relative NOE values for **4**. Values for average NOEs are calculated at 300 K. The values in parentheses give the corresponding results at 600 K.

Proton satd	Proton obsd	Experiment [a]	Minima [b]			$\langle NOE\rangle_{GS}$ $(\langle r^{-6}\rangle)$	$\langle NOE\rangle_{GS}$ $(\langle r^{-3}\rangle^2)$	$\langle NOE\rangle_{MMC}$ $(\langle r^{-6}\rangle)$	$\langle NOE\rangle_{MMC}$ $(\langle r^{-3}\rangle^2)$
			A	B	C				
H-1′	H-2′	1.00	1.00	1.00	1.00	1.00	1.00	1.00 (1.00)	1.00 (1.00)
	H-4	0.75	0.24	0.76	0.01	0.93	0.90	0.63 (0.74)	0.61 (0.73)
	H-3	0.13	0.33	0.17	1.57	0.16	0.15	0.23 (0.24)	0.21 (0.20)
	H-5	0.00	−0.01	−0.01	1.21	−0.01	−0.01	−0.01(−0.01)	−0.01(−0.01)
SD			0.27	0.02	1.00	0.09	0.08	0.08 (0.05)	0.08 (0.04)

[a] Ref. 48; [b] Minimum A: $\phi = -62°$, $\psi = -43°$, $E_{rel} = 0.00$ kcal/mol. Minimum B: $\phi = -37°$, $\psi = -33°$, $E_{rel} = 0.20$ kcal/mol. Minimum C: $\phi = -34°$, $\psi = -161°$, $E_{rel} = 4.06$ kcal/mol. The hydroxymethyl groups are fixed in the *gg* conformation.

deduced from glycosidic linkage conformation variations using simple molecular modelling. Equilibration periods of 2000 macro moves turned out to be sufficient to achieve convergence of running averages of $\langle r^{-6}\rangle_{MMC}$ values.

Theoretical NOEs based upon single minima (NOE_{Min}), averaging over a grid with regular spacing ($\langle NOE\rangle_{GS}$) or by means of the MMC algorithm ($\langle NOE\rangle_{MMC}$), were determined as follows. For the calculation of $\langle NOE\rangle_{GS}$, values only the dihedral angles ϕ and ψ of the glycosidic linkage in question were treated as flexible in order to reduce the number of degrees of freedom. Utilizing the Boltzmann distribution function, ensemble average matrices $\langle r^{-6}\rangle_{GS}$ and $\langle r^{-3}\rangle_{GS}$ were derived; this has been described in detail previously[6,12,13]. During MMC simulations, after each macro move, r^{-6} and r^{-3} matrices corresponding to the actual conformational state were determined. Summation of these matrices over the whole course of the MMC simulation, and calculation of their arithmetic means, as described above, lead to ensemble average matrices $\langle r^{-6}\rangle_{MMC}$ and $\langle r^{-3}\rangle^2_{MMC}$. The matrices $\langle r^{-6}\rangle_{MMC/GS}$ and $\langle r^{-3}\rangle^2_{MMC/GS}$ were subsequently used to construct ensemble average cross relaxation matrices $\langle R\rangle_{MMC}$ or $\langle R\rangle_{GS}$ that finally yielded ensemble average NOEs, $\langle NOE\rangle_{MMC}$, or $\langle NOE\rangle_{GS}$. Single minimum cross relaxation matrices R_{Min} derived from r^{-6}_{Min} values were used to derive NOE_{Min} data. Elements of cross relaxation matrices R_{Min}, R_{GS}, and R_{MMC} were calculated according to the published procedures[30,31].

The decision whether to use a $\langle r^{-6}\rangle$ or a $\langle r^{-3}\rangle^2$ matrix depends on assumptions concerning the relative time scales of internal and overall molecular motions[32]. In both cases, it was assumed that the isotropic rotational correlation time τ_c is identical for all conformational states visited during an MMC simulation or a grid search. Internal motions such as rotations around C-5–C-6 bonds and glycosidic linkages are characterized by internal correlation times τ_i. If interconversion of conformers is fast compared to the overall molecular tumbling ($\tau_i > \tau_c$), as this occurs in large biomolecules such as proteins, it can be shown that $\langle r^{-3}\rangle^2$ values must be used to set up an ensemble average cross relaxation matrix[33–35]. The situation is different for oligosaccharides of such size as **1–4** where molecular tumbling usually takes place in the extreme narrowing limit with τ_c values of the order of 10^{-10} s. Internal motions may still be faster than overall molecular tumbling, but the opposite as well as intermediate cases are plausible. For the opposite case, with internal motions slower than overall molecular tumbling ($\tau_i < \tau_c$), $\langle r^{-6}\rangle$, matrices have to be used[6], and for the intermediate case with $\tau_i = \tau_c$ it can be deduced that the cross relaxation matrix must be constructed from an average[14,33] $(\langle r^{-3}\rangle^2 + \langle r^{-6}\rangle)/2$. Due to lack of experimental evidence, the situation is not clear-cut for oligosaccharides and, therefore, we decided to use both treatments, based upon $\langle r^{-3}\rangle^2$ and $\langle r^{-6}\rangle$ matrices, as done previously[13].

Methyl groups undergo fast internal rotation and require a special treatment. The protocol applied here[31,36] is based on expressions given by Rowan et al.[37].

For the calculation of steady-state NOE values, the series of simultaneous equations derived from the cross relaxation matrix under steady-state conditions[36]

was solved using the Gaussian elimination method:

$$\Sigma_{j \neq k} R_{ij} NOE(j, k) = R_{ik} (i \neq k) \quad (1)$$

where R_{ij} are the elements of the cross relaxation matrix R (R_{Min},$\langle R \rangle_{GS}$ or $\langle R \rangle_{MMC}$), NOE(j, k) is the NOE enhancement factor (NOE_{Min},$\langle NOE \rangle_{GS}$ or $\langle NOE \rangle_{MMC}$) of proton j upon irradiation of proton k. Full matrix $\langle NOE \rangle_{MMC}$ values were calculated every 5000 macro steps, as running averages, in order to allow the calculation of $\langle NOE \rangle_{MMC}$ trajectories that illustrate the development of $\langle NOE \rangle_{MMC}$ values as a function of the number of MMC macro steps.

Motional correlation times τ_c for the calculation of NOEs were assumed to be roughly the same for all four disaccharides and were set at 1.6×10^{-10} s, a value determined earlier by fitting the theoretical Boltzmann-averaged NOEs for **2** to the experimentally determined values[14]. The correlation time τ_i for the internal motion of the *O*-methyl group was set at 1.0×10^{-13} s, a value used in an earlier study of **1** (ref. 31). The same τ values were used for MMC simulations with different temperature parameters. Nuclear relaxation was assumed to be governed by dipole–dipole relaxation and no solvent relaxation effects were taken into account. The absolute NOE values calculated in this fashion were of the same magnitude as those obtained experimentally. For comparison of calculated and experimental NOE data, relative NOEs were determined by setting a suitable intraglycosidic NOE as a reference[31] at 1.0. Only relative NOE values will be reported here (Tables I–IV). A standard deviation (SD) that describes the quality of the fit between experimental and calculated NOEs can be derived for each compound: $SD^2 \equiv 1/N\Sigma_i(NOE_{expt} - NOE_{calcd})^2$, with N being the number of NOEs observed within one disaccharide. These standard deviations are included in Tables I–IV.

Graphical presentations of potential-energy surfaces were performed with the program SURFER running on IBM PCs (or compatible PCs). All scatter plots and visualizations of the results of the MMC simulations were achieved with plotting software[38] written in FORTRAN using the NCAR Graphics library of plot routines (NCAR Graphics, Version 3.00, December 1989, Scientific Computing Division, National Center for Atmospheric Research, Boulder, CO) implemented on an IRIS workstation 4D/50GT.

All calculations were performed either on a Micro-VAX 3500 computer located at the National Research Council in Ottawa or on a Convex C120 computer in the Institute of Biophysical Chemistry in Frankfurt. The CPU time requirements were ~ 48 h for a 250 000 macro step simulation on the Mikro-VAX and ~ 12 h on the Convex. The modified GESA program is available upon request from the authors.

RESULTS AND DISCUSSION

Conformational analysis of glycosidic linkages using the Metropolis algorithm.— The glycosidic linkages under investigation have been the subject of a number of

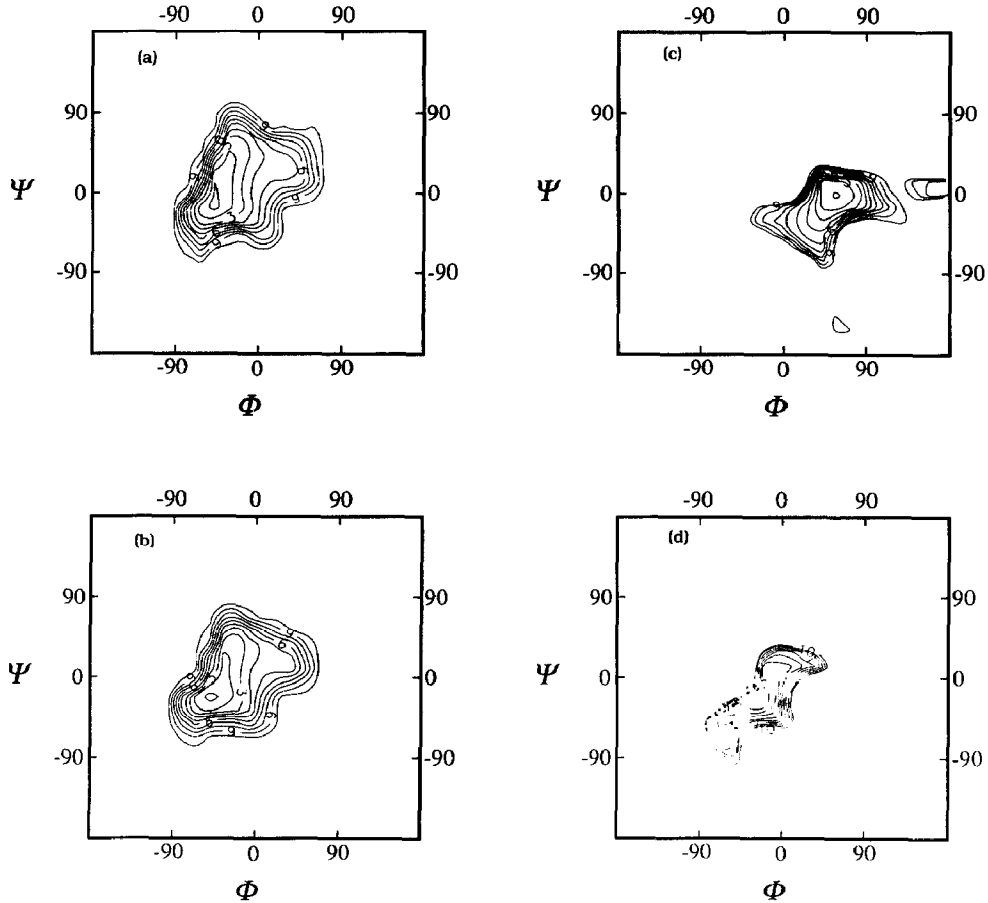

Fig. 1. Potential energy surfaces as a function of ϕ and ψ for **1**–**4**. Isoenergy contours are scaled at 0.5 kcal/mol intervals up to 10 kcal/mol above the global minimum energy: (a) **1**; (b) **2**; (c) **3**; (d) **4**.

previous investigations[12,14,31,39,40–49] and there is significant evidence that these linkages are flexible. Local minima have been detected using relaxed as well as rigid-energy maps[41]. The energy surfaces for the two mannose disaccharides **1** and **2** as their methyl α-glycosides, cellobiose **3** and maltose **4** as their methyl β-glycosides, calculated on the basis of the HSEA force field are shown in Fig. 1. Only dihedral angles ϕ and ψ at the glycosidic linkage in question were varied with the hydroxymethyl groups kept fixed in the *gg* orientation ($\omega = -60°$) and *O*-methyl groups in the conformations found for the global minima ($\phi \approx -50°$, $\psi \approx 60°$ for **1** and **2**; $\phi \approx 50°$, $\psi \approx 60°$ for **3** and **4**). The overall appearance of the potential energy surfaces is very similar to the rigid maps reported in the literature[12,14,41]. Differences occur for the location of the local minima. The values for the ϕ and ψ angles of the global minima, as derived from GESA calculations, are as follows. α-D-Man(1 → 3)-α-D-Man(1 → O)Me **1**: $\phi = -49°$, $\psi = -10°$; α-D-Man(1 → 2)-α-D-Man(1 → O)Me **2**: $\phi = -47°$, $\psi = -20°$; cellobioside **3**: $\phi = 57°$, $\psi = -2°$; mal-

toside **4**: $\phi = -62°$, $\psi = -43°$. ϕ, ψ Coordinates of local minima are given in the footnotes to Tables I–IV. On the basis of the energy surfaces (Fig. 1) ensemble average NMR parameters may be calculated, as has been discussed in detail previously[6,11–13]. A typical run would apply a 10° grid covering the whole conformational space in the ϕ and ψ dimensions. If the energy surface is known in advance, the conformational space sampled may be limited to regions of low energy, allowing a finer grid to be applied. This is of significance because NOEs are dependent on the distribution of inverse sixth moments of interproton distances. The inverse sixth moment distance-dependency also necessitates the sampling of higher energy states, since these may still contribute to the average, given that the corresponding distances are small enough. It has been suggested that an upper limit of 10 kcal/mol above the global minimum is a safe choice for the calculation of ensemble average NOEs[14]. Nevertheless, local minima of low energy have to be located in advance to enable reduction of the grid used for the calculation of ensemble average values. This gains importance with a growing dimensionality of the conformational space in question. The MMC sampling offers an attractive way for overcoming this problem. Instead of "manually" determining low-energy areas in conformational space, a probability function is used that automatically guarantees sampling of low-energy parts. Several functions[50] are known that achieve this goal, but the most widely used is the Metropolis function[28] that compares a random number to the Boltzmann factor $\exp(-\Delta E/RT)$ to decide whether a move in conformational space is accepted. In this manner, a Markov chain of conformational states is generated, ensuring that each state is visited according to its proper statistical weight, as already explained. During the MMC simulation, the low-energy parts of the energy hyperspace are sampled, whereas the very high-energy parts are virtually never reached. The parts of the energy surfaces of the four disaccharides covered during the 250 000 macro step simulations are shown in Fig. 2 as scatter plots. Dots mark the coordinates in ϕ,ψ space that have been visited by the saccharides and, consequently, dark shading indicates a high population of conformers within this range of ϕ,ψ values. The plots are complementary to the energy surfaces in Fig. 1. It is important to notice that the scatter plots contain additional information as compared to the potential energy-surfaces, as they represent a projection of the six-dimensional conformational space into the two dimensions spanned by the dihedral angles ϕ and ψ at the glycosidic linkage in question. This allows a convenient representation of conformational spaces of high dimensionality, and especially gives the opportunity for study of the conformational effects of branching, an issue of particular importance, for instance, in the case of a high-mannose type undecasaccharide[51] or of xyloglycan[52].

For **1–4**, convergence of running averages of NOEs was monitored utilizing the interglycosidic $\langle r^{-6} \rangle$ values for the distances H-1′–H-3 in **1**, H-1′–H-2 in **2**, and H-1′–H-4 in **3** and **4** (see also Computational methods). Fig. 3 shows the development of these values with the number of MMC macro steps during the equilibra-

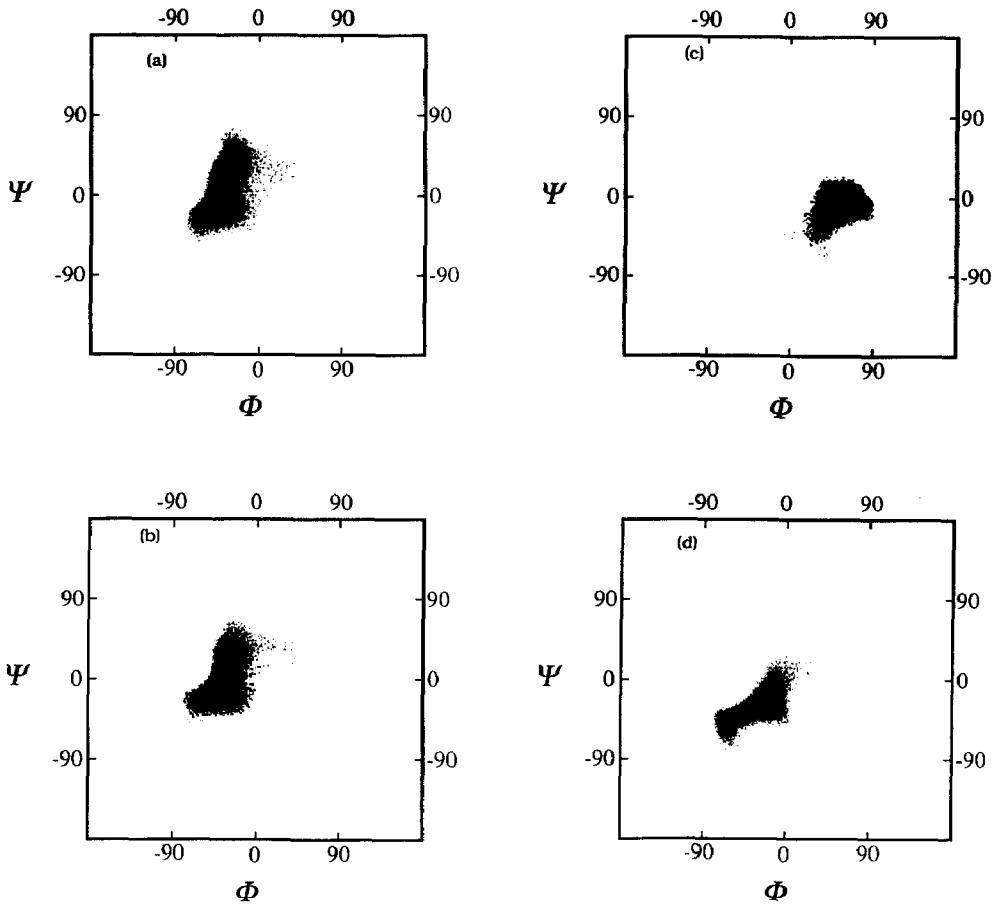

Fig. 2. Scatter plots resulting from 250000 macro step MMC simulations for **1–4** with the temperature parameter set at 300 K (a–d) or 600 K (e and f): (a and e) **1**; (b) **2**; (c and f) **3**; (d) **4**. In all cases the maximum step length was chosen as 20° leading to an overall acceptance ratio of ~ 0.3 at 300 K and 0.4 at 600 K.

tion period. In all cases, the starting dihedral angles at the glycosidic linkages were set at $\phi = \psi = 0°$. It is evident from Fig. 3 that the $\langle r^{-6} \rangle$ values have converged after 1000–2000 macro steps. The curves in Fig. 3 indicate that the rate of approaching an equilibrium state is different depending on the glycosidic linkage. For **4** (Fig. 3d) the approach is slowest and the fluctuations of $\langle r^{-6} \rangle$ are most pronounced. This observation is explained by the characteristic shape of the potential-energy surface of this disaccharide where two conformationally closely related main minima (minima A and B, see Table IV) are separated by a low energy barrier of < 2 kcal/mol (see also discussion later). For **3** (Fig. 3c) the approach is rather fast due to the symmetrical shape of the potential-energy surface in the global minimum region (compare Figs. 1c and 2c, and the corresponding discussion later). The selected $\langle r^{-6} \rangle$ value for **1** (Fig. 3a) converges

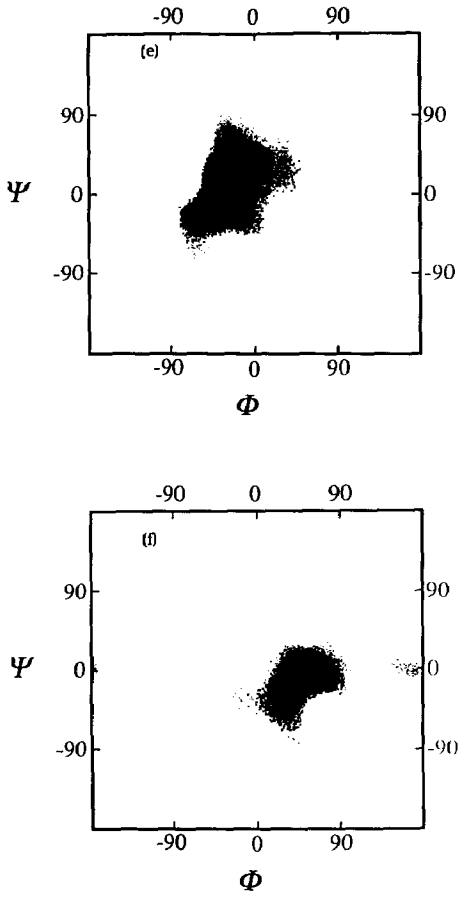

Fig. 2. (continued).

somewhat more slowly towards an equilibrium value than found for **3**. A very similar rate of convergence is observed for **2** (Fig. 3b), reflecting the similar shape of the corresponding energy surfaces of **1** and **2** (see Figs. 1a and 1b).

The choice of the starting conformation is not very critical for **1–4** if the ϕ,ψ coordinates are not too far away from the global minimum coordinates. Deviations of 50° from the global minimum in both directions ϕ and ψ usually are not harmful. However, starting from very distant points on the energy surface may trap the disaccharide in a high energy local minimum. For instance, a simulation of the α-(1 → 2)-linked **2** at 300 or 600 K starting from $\phi = \psi = 150°$ (Fig. 4b, region S) does not carry the molecule towards the region of the global minimum during an equilibration period of 2000 macro steps. The disaccharide is trapped in a local minimum around $\phi = 0°$ and $\psi = 180°$ (Fig. 4b, region L) that has an energy of ~ 50 kcal/mol (Fig. 4a). However, a MMC simulation at 2000 K drives the molecule into the region of the global minimum (Fig. 4b, region G). After ~ 1600 macro moves, the energy drops from 50 to < 0 kcal/mol (compare (Fig. 4a to Fig.

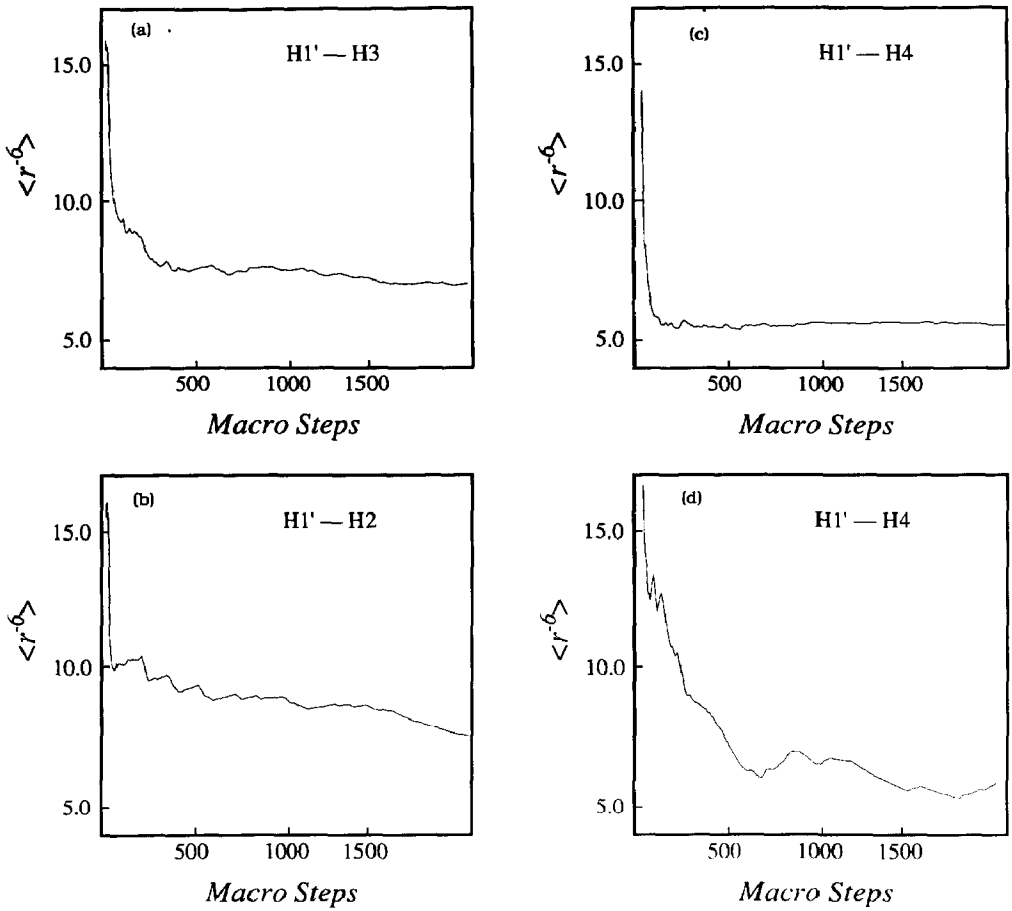

Fig. 3. Development of interglycosidic $\langle r^{-6} \rangle$ values during the equilibration period (2000 MMC macro steps). The corresponding proton pairs are indicated and selected as the ones giving rise to the most prominent interglycosidic: (a) **1**; (b) 2; (c) **3**; (d) **4**. In each case the starting conformation of the glycosidic linkage in question was $\phi = \psi = 0°$ with a potential energy > 1000 kcal/mol above the minimum.

4b) placing **2** in the global minimum region. Thus, it is advisable to start the simulation not too far away from the global minimum. In practice, it turned out that a rough estimate for the starting conformation is sufficient for **1–4**. In the case of more complex oligosaccharide structures, a careful selection of starting conformations is required[52,53]. For instance, in the case of a high-mannose type undecasaccharide, where the ϕ, ψ, and ω angles span a 31-dimensional conformational space, we first performed short (2000 macro moves) MMC simulations at 2000 K with ϕ, ψ, and ω angles set at starting values corresponding to global and local minima of the constituent disaccharides[51]. Subsequently, regions of low energy were used as starting points for the refinement of energetically favorable conformers, utilizing the Davidon–Fletcher–Powell algorithm[54] of the GESA program. The method described is based upon the idea of "simulated annealing"[55]. If a

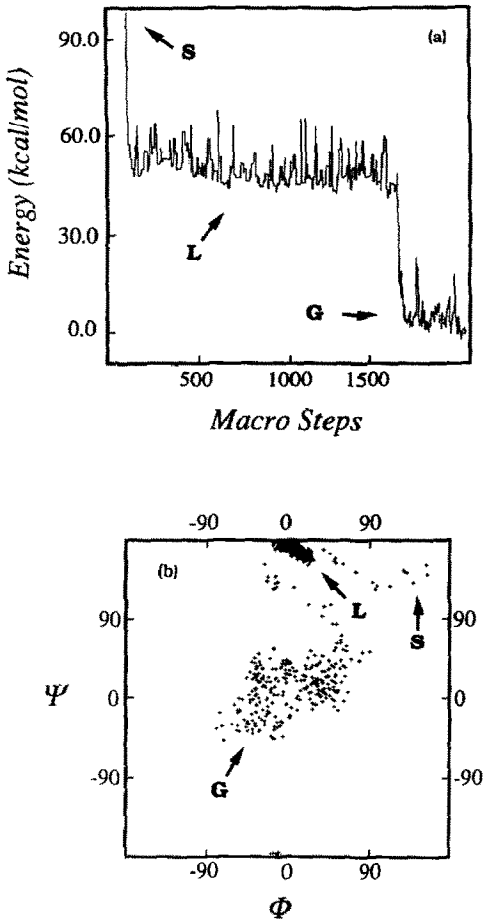

Fig. 4. 2000 macro step MMC simulation of **2** at 2000 K: (a) potential energy as a function of the number of macro steps; (b) scatter plot showing the path from the starting conformation at $\phi = \psi = 150°$ towards the global minimum region; S, L, and G indicate the starting point of the simulation, the region of the local minimum, and the region of the global minimum, respectively.

conventional grid search with a grid of 10° resolution were used to perform these calculations, the number of conformational states to be calculated would be 36 (ref. 31). Even assuming that it is possible to decrease the regions of conformational space to be sampled prior to averaging over desired properties, grid-search techniques cannot adequately handle a problem of this complexity.

The energy surfaces of **1** and **2** pose no difficulties to the simulation in terms of energy barriers that would have to be surmounted. In both cases, the scatter plots resulting from the MMC simulation at 300 K are superposable with the corresponding energy surfaces, indicating that the additional variable dihedral angles which are "projected" into the two dimensions of the scatter plots in Figs. 2a and 2b do not interfere significantly with the glycosidic linkages in question. The local acceptance ratio fluctuates only very little throughout the whole MMC simulation.

A corresponding simulation, carried out at 600 K, leads as expected to a wider distribution of conformational states, as shown for **1** in Fig. 2e. This effect will be discussed in conjunction with experimental NOEs in order to determine the relevance of such a widening of the energy surface on the magnitude of theoretical ensemble average NOEs.

Simulations at 300 K show that during the 250000 MMC macro steps, **3** cannot overcome the energy barrier between the global minimum at $\phi = 60°$ and $\psi = 0°$ (minimum A in Table III), and the local minimum at $\phi = 168°$ and $\psi = 0°$ (minimum B in Table III). From inspection of Fig. 1c in comparison to Fig. 2c, it is clear that the disaccharide does not cross the barrier. This problem can be solved by performing the simulation at an elevated temperature and comparing the results to those obtained at 300 K. A scatter plot for the simulation at 600 K (Fig. 2f) shows that the region of local minimum B is now populated (compare also the potential-energy surface for **3** in Fig. 1c). At 600 K, the energy barrier of more than 10 kcal/mol is surmounted six times (indicated by arrows in Fig. 5a). A plot of ϕ as a function of the number of macro steps (Fig. 5a) clearly shows, however, that the molecule resides only for a very short period of the whole MMC simulation in local minimum B, thus contributing little to any observable average quantity. The different potential-energy surface characteristic of the global minimum and local minimum B are well illustrated by a plot of the local acceptance ratio as a function of the number of macro steps (Fig. 5b): a sharp drop in the acceptance ratio is detected after a transition from the global minimum to local minimum B has been made, indicating steeper gradients of the energy well of local minimum B. Two other local minima are found in the rigid map of **3** with ϕ, ψ values of 59°, −146° (minimum C in Table III) and 28°, 173° (minimum D in Table III). Only minimum C can be seen in the energy surface in Fig. 1c; minimum D is too steep to be caught by the contouring algorithm. However, it shows up on the energy surface when plotting contour lines up to 20 kcal/mol instead of 10 kcal/mol (data not shown). These two minima are not visited during either MMC simulation at 300 or 600 K. From the foregoing discussion, it should be clear that the importance of these minima for the calculation of any average quantity should be negligible. Thus, no attempts were undertaken to optimize the parameters used in the MMC simulation in order to move the molecule into the region of minima C or D.

The simulation of **4** offers fewer difficulties. As seen from Fig. 1d, there is a double minimum that may also be regarded as one broad minimum since the energy barrier between the two minima A (Table IV, ϕ, $\psi = -62°$, $-43°$, $E_{rel} = 0.00$ kcal/mol) and B (Table IV, ϕ, $\psi = -37°$, $-33°$, $E_{rel} = 0.20$ kcal/mol) is < 2 kcal/mol. The 10 kcal/mol border of these two main minima stretches in a range of $\sim 150°$ in both dimensions ϕ and ψ. A local minimum may be detected upon inspecting the rigid map in Fig. 1d at ϕ, $\psi = -34°$, $-161°$ (Table IV, minimum C, $E_{rel} = 4.06$ kcal/mol). Since this local minimum is not only high in energy but also covers only a small range of the ϕ, ψ map, its contribution to overall average

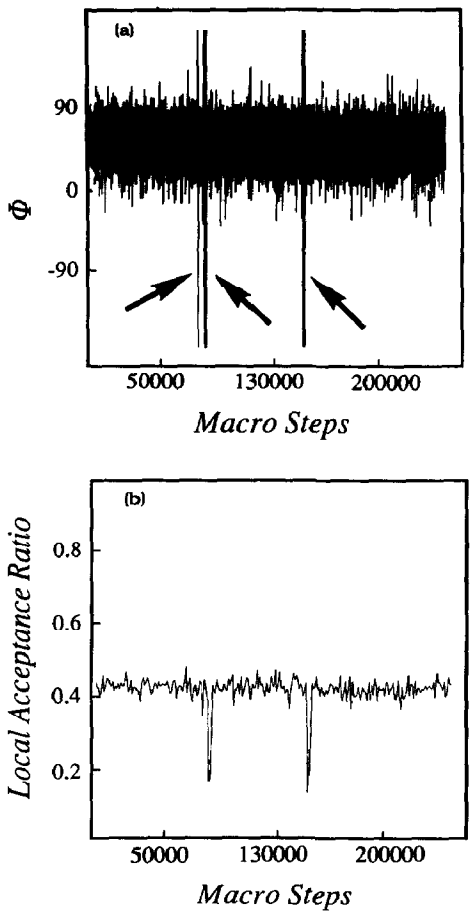

Fig. 5. 250000 macro step MMC simulation of 3 at 600 K: (a) dihedral angle ϕ at the β-(1 → 4)-glycosidic linkage as a function of the number of macro steps (six transitions between the global and the local minimum are observed as indicated by the arrows); (b) local acceptance ratio as a function of the number of macro steps.

quantities may be considered unimportant. From Fig. 2d it can be seen that the low-energy areas of the energy surface (Fig. 1d) embracing minima A and B are sampled at 300 K. Elevating the temperature to 600 K does not substantially increase the extent of the energy surface sampled as observed for cellobiose. This reflects the fact that maltose contains a more rigid glycosidic linkage than cellobiose, as described in earlier communications[41]. An important point to mention is that the conformation of the α-(1 → 4) linkage between the two glucose residues has a significant steric influence on the ease of rotation of the hydroxymethyl group of the reducing glucose residue. Following the conformations of the two hydroxymethyl groups as a function of the number of MMC macro steps, it may be seen that more transitions between *gg*, *gt*, and *tg* conformations during a given

number of macro moves are observed for the hydroxymethyl group in the (1 → 4)-linked glucose unit as compared to the terminal glucose unit.

MMC simulations of a high-mannose type undecasaccharide that has been the subject of recent studies[56,57] indicated that the whole conformational space was sampled, and a good agreement with NMR experimental data was obtained. The undecasaccharide mentioned is a highly branched structure including ten glycosidic and eleven C-5–C-6 bonds, resulting in a 31-dimensional conformation space. A detailed analysis of this undecasaccharide, including the simulation of experimental NOE data and vicinal ^1H–^1H coupling constants[56,57], is beyond the scope of this publication and will be given elsewhere[51].

Comparison of the Metropolis Monte Carlo simulations with experimentally derived NOE values.—Steady-state NOE experimental data have been published on derivatives of **1–4** (refs. 14, 31, 45, 48). Reliable quantitative data for steady-state NOEs are difficult to obtain because of overlapping signals and spin systems of higher order. The emphasis of this investigation is on the assessment of the MMC algorithm in comparison to a systematic grid-search method, both based on the HSEA force field. The calculated data are related to NOE values obtained from single minimum models, thus shedding light on the question of how sensitive are NOE values to molecular motion. In order to facilitate a comparison of theoretical NOEs derived via different methods, for each compound "standard deviations" SD (cf. Computational methods) of theoretical NOEs from the experimental values are calculated and included in Tables I–IV.

The α-(1 → 3)-linked mannose disaccharide glycoside (**1**) has been the subject of a number of investigations[12,31,39,43]. It appears that the best agreement between experimental and theoretical data can be obtained by applying the HSEA force field, together with Boltzmann-averaging[39]. Relaxed energy maps have been calculated using a modified version of the MM2 force field[58], MM2CARB[59]. Recently, the AMBER force field[60,61], as provided by the molecular modelling package DISCOVER (Biosym Technologies Inc.) with a parametrization for carbohydrates[62], was used in a molecular dynamics (MD) simulation of the trisaccharide α-D-Man(1 → 3)-β-D-Man(1 → 4)-β-D-GlcNAc (ref. 43). The results obtained from these previous studies, as well as those from the MMC simulations, the Boltzmann averaging and the NOE data derived from the global minimum conformation of **1** are summarized in Table I. It is obvious that the introduction of flexibility around the glycosidic linkage into the molecular model causes an improvement of the fit between experimental and theoretical data. The results of both experiments, irradiation of H-1′ as well as irradiation of H-2, are approached more closely by the theoretical values derived on the basis of Boltzmann averaging, regardless of the underlying force field. Inspecting the values for the H-2 irradiation experiment (Table I) reveal differences for the calculated values of the NOE enhancement of H-5′, depending on the method used. This is explained by the fact that rotation of the hydroxymethyl group influences the relaxation of H-5′. For the calculation of NOE values from the global minimum and those derived from statistical-mecha-

nics averaging, the hydroxymethyl groups were fixed in the *gg* conformation and thus do not take any motion at all into account. For the MMC simulations, the C-5–C-6 side chains were allowed to rotate. No extra torsional potential function was applied for the rotation of the hydroxymethyl groups, since none of the models used so far has been capable of reproducing these side chain motions with sufficient reliability. It is anticipated that the use of a suitably parametrized torsional potential function for the rotation around C-5–C-6 bonds in hexopyranoses will improve this situation. Elevating the temperature in the MMC simulation to 600 K (values in parentheses in Table I) does not change the predicted NOE values dramatically. Only the NOE of H-5′, observed upon irradiation of H-2, is seen to be affected. This can be attributed to a more equal distribution of C-5–C-6 rotamers in the ante-terminal mannose unit at the elevated temperature. Comparing the data derived from Boltzmann averaging utilizing a systematic grid search to those calculated with the MMC algorithm reveals that there are small differences, which have to be attributed to the fact that the grid applied for the statistical mechanics calculations is too coarse, and also that rotation around the C-5–C-6 axes was not taken into account for the systematic grid-search calculations. In theory, both results should be the same and the application of a very fine grid can be used to show that both methods are indeed equivalent[63].

Similar conclusions may be drawn for the corresponding α-(1 → 2)-linked mannosyl disaccharide **2**. It has been shown that the systematic grid search approach, with the HSEA force field, has been successful in modelling experimentally derived NOE data for **2** (ref. 14). Also, an MD simulation, employing the modified AMBER force field[43] has been performed for **2** as part of a larger structure and the values obtained in that study were compared to 2D-NOE data from more-complex structures[40]. A comparison of our results with the MD derived data was not attempted since the present study deals with steady state NOEs. The interglycosidic NOEs at the α-(1 → 2) linkage are sensitive towards molecular motion around this bond, as shown previously[14,40], and is also apparent from examination of Table II. The calculations again show that MMC calculations are equivalent to Boltzmann averaging (Table II), with the restrictions pointed out above for **1**. The NOE experiments, in which H-1′, H-2′, and H-2 are saturated, yield results that are reproduced better by the MMC simulation or the Boltzmann averaging than by the global minimum single state model. Irradiation of H-1 induces an NOE enhancement of H-5′ that depends on the orientation of the hydroxymethyl group attached to C-5′. The MMC simulations performed at 600 K yield NOE values that are rather similar to those derived at 300 K. The only significant change of a calculated NOE is observed for the NOE of H-5′ upon irradiation of H-1: the best fit between experimental and theoretical data is achieved for the MMC simulation performed at 600 K with the NOEs calculated from the relaxation matrix based upon $\langle r^{-3}\rangle^2_{MMC}$ values. The sensitivity of this particular NOE to the temperature parameter is due to the dependence on the rotamer distribution of the hydroxymethyl group[64].

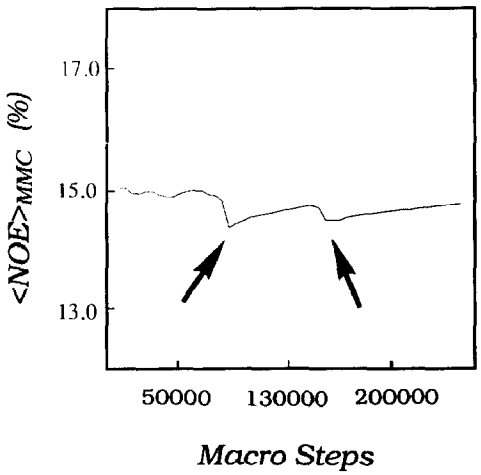

Fig. 6. Interglycosidic $\langle NOE \rangle_{MMC}$ value (running average) for the proton pair H-1′–H-4 of **3** as a function of the number of MMC macro steps at 600 K. The positions where the molecule enters the local minimum at $\phi = 168°$, $\psi = 0°$ are indicated with an arrow.

For methyl β-cellobioside **3**, both the global minimum (minimum A in Table III) and the local minimum at ϕ, $\psi = 168°$, 0° (minimum B in Table III) are sampled when performing a MMC simulation at 600 K (Fig. 2f). At 300 K, only the global minimum region is covered (Fig. 2c). We calculated $\langle NOE \rangle_{MMC}$ values both at 300 and at 600 K, and compared the results in order to evaluate the significance of such local minimum conformers for the average NOEs. First, inspection of Table III reveals that $\langle NOEs \rangle_{GS}$ obtained from Boltzmann averaging do not differ significantly from the global minimum NOEs (minimum A in Table III). The influence of the temperature parameter change from 300 to 600 K on the magnitude of the $\langle NOE \rangle_{MMC}$ values is too small to be verified experimentally (Table III). To illustrate this more clearly, a plot of the magnitude of the running average interglycosidic $\langle NOE \rangle_{MMC}$ between H-1′ and H-4 as a function of the number of MMC macro steps (Fig. 6) shows that when the molecule moves into the local minimum there is a small drop in $\langle NOE \rangle_{MMC}$ values (marked with arrows in Fig. 6). Since the molecule only resides for a very short period in the local minimum, this drop is levelled out again relatively soon after the molecule has arrived back in the global minimum region (Fig. 5). Thus, the contribution of local minimum conformers towards the overall average values of NOEs is rather small.

Positive NOEs are observed for H-3 and H-5 upon irradiation of H-1′ (ref. 45), and it has been argued that they cannot be explained[45] by the so called "three-spin effect"[30] but rather by the presence of such conformers as C and D (see Table III). Since the experimental NOE values given in the literature[45] consist of the sum of the enhancements of H-3, H-6a, and H-6b when irradiating H-1′, Table III contains only this sum. It should be noted that the NOEs of H-3 and H-5 are

dependent[65] on both the choice of the conformer (cf. Table III, conformers A–D) and on the overall motional correlation time τ_c. Calculations of the NOEs of H-3 and H-5 with different correlation times τ_c clearly indicate that the signs of both NOEs change from negative to positive as a function of τ_c, without applying Boltzmann averaging. τ_c values larger than 2.5×10^{-10} s at 250 MHz caused positive NOEs of H-3 and H-5 in all cases. This means that relatively slight variations of τ_c may induce the same effect as would the presence of small amounts of conformers C and D, and thus care has to be taken when arguing in favour of a significant contribution of conformers C and D to the conformational equilibrium at the glycosidic linkage in **3**. The NOE values obtained from the MMC simulation and from Boltzmann averaging are comparable.

At first sight, examination of Table IV may suggest that for **4** minimum B is the one that is most closely reproducing the experimental data. However, from the preceding discussion it becomes clear that this minimum is not the only one present, which has already been pointed out[44]. The global minimum A which is separated from minimum B only by a very low energy barrier (~ 2 kcal/mol) reproduces the experimental data less well. Minimum C is too high in energy to contribute significantly to experimentally observed NOE values. The MMC simulations of **4** at 300 and 600 K cover the regions of minima A and B but do not sample minimum C. The $\langle NOE \rangle_{MMC}$ values derived from these simulations also give a close fit between experimental and theoretical data, with the fit apparently being slightly better at 600 K (Table IV). The grid-search method yields $\langle NOE \rangle_{GS}$ values that are comparable to the MMC derived values but the fit with the experimental data is less good. Again, this is due to the limited resolution of the grid used.

Especially in the case of **4**, it is seen that the interglycosidic NOE between H-1′ and H-4 is very susceptible to small changes of the glycosidic linkage conformation. This has been discussed above for the dependence of the $\langle r^{-6} \rangle_{MMC}$ value for this proton–proton distance, as a function of the number of macro moves (Fig. 3d). Jumping between the two structurally closely related minima A and B (see Table IV) caused significant fluctuations of $\langle r^{-6} \rangle_{MMC}$ and consequently the approach towards equilibrium was observed to be slowest for **4** compared to **1**, **2**, and **3**. We conclude from these results that in this case the interglycosidic NOE between H-1′ and H-4 is a sensitive measure of motions around the glycosidic linkage. Nevertheless, one has to keep in mind that the experimental NOE data[48] have an estimated error margin of 20–30%. For a rigorous quantitative treatment, more accurate experimental data are desirable. Very slight changes in the conformation at the glycosidic linkage easily worsen the perfect fit for any global minimum conformer (compare the NOEs for conformers A and B in Table IV) and thus the good fit between MMC derived $\langle NOE \rangle$ values and experimental data must be considered more significant. In this context, it is interesting to note that recently NOE data have been published[66] on a *C*-glycosyl derivative of maltose, suggesting that the conformational behaviour of this compound is very similar to that of maltose.

CONCLUSIONS

The studies performed show that MMC simulations provide a convenient method for the calculation of ensemble average NOEs in saccharides. For **1–4** ensemble average NOEs were calculated using MMC simulations as well as simple Boltzmann averaging on the basis of a systematic grid search. As expected, both methods give the same results with small deviations resulting from a limited grid density. The advantage of the MMC method for the computation of NOEs across glycosidic linkages lies in the ease with which additional variables of the restricted conformational space, such as torsions around C-5–C-6 bonds or C–O bond rotations of methylated sugar hydroxyls may be encompassed. The scatter plots (Fig. 2) derived for the individual glycosidic linkages in **1–4** contain additional information as compared to the corresponding potential energy surfaces (Fig. 1) because they represent projections of the complete six-dimensional conformational space into the two dimensions spanned by the dihedral angles ϕ and ψ at the glycosidic linkage in question. The ensemble average NOEs for **1–4** gave a better fit with experimental NOEs than corresponding values derived on the basis of single conformation models.

The temperature effects on the calculations suggest that the temperature may be used as an artificial parameter to allow easier jumping between different local minima. It will have to be investigated whether it is appropriate to run simulations at elevated temperatures since this may give a closer fit with experimental data (cf. Tables I–IV). In this context it should also be noted that the underlying HSEA force-field does not predict small islands of low energy such as those originally observed for maltose[67] or as seen for the α-D-Man(1 $\rightarrow$ 3)-α-D-Man unit in a crystalline complex between a lectin and an octasaccharide[68]. Further research will be necessary to identify the general importance of such narrow local minima. Since all calculations were made assuming isotropic motion, we also emphasize that reorientation of even small disaccharides is not completely isotropic[69] and it may well be that the inclusion of anisotropy effects into MMC simulations will further improve the calculated data. This problem certainly provides another subject of interest for future research in the field.

Finally, some aspects that should be considered when comparing the MMC method described to the widely-used MD approach, that has been especially successful in modelling protein conformations[70,71], must be mentioned. Compared to MD calculations, MMC simulations have the advantage that systems with varying correlation times of local motions[17] can be treated with greater ease. This can become important for oligosaccharides when comparing molecular motions at glycosidic linkages to side-chain motions. The respective correlation times are not necessarily of the same order of magnitude. In MD simulations, it is necessary to choose the integration-time step according to the characteristic time of the fastest motion and subsequently integrate up to the relaxation time of the slowest motions[17]. Another feature of the MMC method is that it samples canonical

(constant temperature) ensembles, whereas conventional MD techniques work at constant energy (microcanonical ensemble). Special precautions, such as coupling to a heat bath, are required in MD for sampling of canonical ensembles. Thus, if the main interest is in the prediction of time-independent ensemble average values MMC simulations will offer an attractive alternative to MD methods.

ACKNOWLEDGMENTS

The collaboration between T.P. and J.R.B. was financed by a NATO research grant CRG.890356. T.P. thanks the Deutsche Forschungsgemeinschaft for a grant within the Sonderforschungsbereich 169. This work was supported in part by grants from the National Institutes of Health (1-P41-RR05351-01) and the advanced computational methods center of the University of Georgia (to R.S.P. and B.M.). We wish to thank Professor Klaus Bock for generous hospitality at the Carlsberg Laboratory, Copenhagen, and for discussions of the simulation method described. We also appreciate the continuous encouragement of Dr. David Bundle, National Research Council of Canada, who accompanied the project at all stages of its development. Professor Heinz Rüterjans, Institute of Biophysical Chemistry, University of Frankfurt, is thanked for providing access to the computing facilities in his laboratory.

REFERENCES

1 R.U. Lemieux, *Chem. Soc. Rev.*, 18 (1989) 347–374.
2 M. Cygler, D.R. Rose, and D.R. Bundle, *Science*, 253 (1991) 442–445.
3 B. Meyer, in J. Thiem (Ed.), *Topics in Current Chemistry*, Vol. 154 Springer-Verlag, Berlin, 1990, pp 141–208.
4 K. Bock, *Pure Appl. Chem.*, 55 (1983) 605–622.
5 K. Wüthrich, *NMR of Proteins and Nucleic Acids*, Wiley, New York, 1986.
6 D.A. Cumming and J.P. Carver, *Biochemistry*, 26 (1987) 6664–6676.
7 H. Thøgersen, R.U. Lemieux, K. Bock and B. Meyer, *Can. J. Chem.*, 60 (1982) 44–57.
8 A. Parfondry, N. Cyr, and A.S. Perlin, *Carbohydr. Res.*, 59 (1977) 299–309.
9 K. Bock, A. Brignole, and B.W. Sigurskjold, *J. Chem. Soc., Perkin Trans.*, (1986) 1711–1713.
10 L. Poppe and H. van Halbeek, *J. Am. Chem. Soc.*, 113 (1991) 363–365.
11 D.A. Cumming and J.P. Carver, *Biochemistry*, 26 (1987) 6676–6683.
12 A. Imberty, V. Tran, and S. Pérez, *J. Comput. Chem.*, 11 (1989) 205–216.
13 T. Peters, J.-R. Brisson, and D.R. Bundle, *Can. J. Chem.*, 68 (1990) 979–988.
14 T. Peters, *Liebigs Ann. Chem.*, (1991) 135–141.
15 K. Binder and D. Stauffer, in K. Binder (Ed.), *Topics in Current Physics: Applications of the Monte Carlo Method in Statistical Physics*, Vol. 36, Springer-Verlag, Berlin, 1987, pp. 1–36.
16 M.P. Allen and D.J. Tildesley, *Computer Simulation of Liquids*, Clarendon Press, Oxford, 1989.
17 K. Binder and D.W. Heermann, in P. Fulde (Ed.), *Springer Series in Solid-State Sciences: Monte Carlo Simulation in Statistical Physics*, Vol. 80, Springer-Verlag, Berlin , 1988.
18 Z. Li and H.A. Scheraga, *Proc. Natl. Acad. Sci. U.S.A.*, 84 (1987) 6611–6615.
19 K.D. Gibson and H.A. Scheraga, in M. H. Sarma and R.H. Sarma (Eds.), *Structure and Expression: Vol. I, From Proteins to Ribosomes*, Adenine Press, Guilderland, NY, 1988, pp 67–94.
20 D.R. Ripoll and H.A. Scheraga, *Biopolymers*, 30 (1990) 165–176.
21 A. Duben and C.A. Bush, *Proc. Summer Comput. Simul. Conf.*, (1982) 449–452.
22 D.A. Rees and P.J.C. Smith, *J. Chem. Soc., Perkin Trans. 2*, 8 (1975) 830–835.

23 D.A. Rees and P.J.C. Smith, *J. Chem. Soc., Perkin Trans. 2*, 8 (1975) 836–840.
24 R.C. Jordan, D.A. Brant, and A. Cesaro, Biopolymers, 17 (1978) 2617–2632.
25 A. Cesaro and D.A. Brant, *ACS Symp. Ser.*, 150 (1981) 513–527.
26 B. Meyer, *Int. Carbohydr. Symp.* (1982) Vancouver, Abstr. II/25; H. Paulsen, T. Peters, V. Sinnwell, R. Lebuhn, and B. Meyer, *Liebigs Ann. Chem.*, (1984) 951–976.
27 G.A. Jeffrey, R.K. McMullan, and S. Takagi, *Acta Cryst., Sect. B*, 33 (1977) 728–733.
28 N. Metropolis, A.W. Rosenbluth, M.N. Rosenbluth, A.H. Teller, and E. Teller, *J. Chem. Phys.*, 21 (1953) 1087–1092.
29 W. Chapman and N. Quirke, *Phys. Status Solidi B*, 131 (1985) 34–40.
30 J.H. Noggle, and R.E. Schirmer, *The Nuclear Overhauser Effect*, Academic Press New York, 1971.
31 J.-R. Brisson and J.P. Carver, *Biochemistry*, 22 (1983) 1362–1368.
32 J. Tropp, *J. Chem. Phys.*, 72 (1980) 6035–6043.
33 H. Kessler, C. Griesinger, J. Lautz, A. Müller, W.F. van Gunsteren, and H.J. Berendsen, *J. Am. Chem. Soc.*, 110 (1988) 3393–3396.
34 D. Neuhaus and M.P. Williamson, *The Nuclear Overhauser Effect in Structural and Conformational Analysis*, VCH-Verlagsgesellschaft, Weinheim, 1989.
35 A.E. Torda, R.M. Scheek, and W.F. van Gunsteren, *Chem. Phys. Lett.*, 157 (1989) 289–294.
36 F. Heatley, L. Akhter, and R.T. Brown, *J. Chem. Soc., Perkin Trans. 2*, (1980) 919–924.
37 R. Rowan, J.A. McCammon, and B.D. Sykes, *J. Am. Chem. Soc.*, 96 (1974) 4773–4780.
38 T. Peters, *Plotting Software*, (1991) unpublished.
39 J.P. Carver, D. Mandel, S.W. Michnik, A. Imberty, and J.W. Brady, *ACS Symp. Ser.*, 430 (1990) 266–280.
40 J.C. Edge, U.C. Singh, R. Bazzo, G.L. Taylor, R.A. Dwek, and T.W. Rademacher, *Biochemistry*, 22 (1983) 1971–1974.
41 A.D. French, *Carbohydr. Res.*, 188 (1989) 206–211.
42 S.N. Ha, L.J. Madsen, and J.W. Brady, *Biopolymers*, 27 (1988) 1927–1952.
43 S.W. Homans, *Biochemistry*, 29 (1990) 9110–9118.
44 R.U. Lemieux and K. Bock, *Arch. Biochem. Biophys.*, 221 (1983) 125–134.
45 G.M. Lipkind, A.S. Shashkov, and N.K. Kochetkov, *Carbohydr. Res.*, 141 (1985) 191–197.
46 S. Melberg and K. Rasmussen, *Carbohydr. Res.*, 69 (1979) 27–38.
47 S. Melberg and K. Rasmussen, *Carbohydr. Res.*, 71 (1979) 25–27.
48 A.S. Shashkov, G.M. Lipkind, and N.K. Kochetkov, *Carbohydr. Res.*, 147 (1986) 175–182.
49 V. Tran, A. Buleon, A. Imberty, and S. Pérez, *Biopolymers*, 28 (1989) 679–690.
50 H. Müller-Krumbhaar and K. Binder, *J. Stat. Phys.*, 8 (1973) 1–7.
51 T. Peters, unpublished work.
52 S. Levy, W.S. York, R. Stuike-Prill, B. Meyer, and L.A. Staehelin, *Plant J.*, 1 (1991) 195–215.
53 B. Meyer, M. Zsiska, and R. Struike-Prill, in D.P. Landau, K.M. Mon, and H.B. Schuttler (Eds.), *Computer Simulations in Condensed Matter Physics IV*, Springer-Verlag, Berlin, 1991, in press.
54 R. Fletcher and M.J.D. Powell, *Comput. J.*, 6 (1963) 163–167.
55 S. Kirkpatrick, C.D. Gelatt Jr., and M.P. Vecchi, *Science*, 220 (1983) 671–673.
56 S.W. Homans, R.A. Dwek, J. Boyd, M. Mahmoudian, W.G. Richards, and T.W. Rademacher, *Biochemistry*, 25 (1986) 6342–6350.
57 S.W. Homans, A. Pastore, R.A. Dwek, and T.W. Rademacher, *Biochemistry*, 26 (1987) 6649–6655.
58 N.L. Allinger, *J. Am. Chem. Soc.*, 99 (1977) 8127–8134.
59 I. Tvaroska and S. Pérez, *Carbohydr. Res.*, 149 (1986) 389–410.
60 S.J. Weiner, P.A. Kollman, D.T. Nguyen, and D.A. Case, *J. Comput. Chem.*, 7 (1986) 230–252.
61 S. Weiner, P.A. Kollman, D.A. Case, U. Chandra Singh, C. Ghio, G. Alagona, S.P. Profeta and P. Weiner, *J. Am. Chem. Soc.*, 106 (1984) 765–784.
62 S.N. Ha, A. Giammona, M. Field, and J.W. Brady, *Carbohydr. Res.*, 180 (1988) 207–221.
63 B. Meyer, unpublished work.
64 R. Stuike-Prill and B. Meyer, *Can. J. Chem.*, (1991) submitted.
65 K. Bock, H. Lönn, and T. Peters, *Carbohydr. Res.*, 198 (1990) 375–380.
66 Y. Wang, P.G. Goekjian, D.M. Ryckman, W.H. Miller, S.A. Babirad, and Y. Kishi, *J. Org. Chem.*, 57 (1992) 482–489.
67 S. Pérez and C. Vergelati, *Polym. Bull.*, 17 (1987) 141–148.

68 A. Imberty, M.M. Delage, Y. Bourne, C. Cambillau, and S. Pérez, *Glycoconjugate J.*, 8 (1991) 456–483.
69 J.M. Berry, L.D. Hall, and K.F. Wong, *Carbohydr. Res.*, 56 (1977) c16–c20.
70 W.F. van Gunsteren, *Molecular Simulation*, 3 (1989) 187–198.
71 W.F. van Gunsteren and J.C. Berendsen, *Angew. Chem.*, 102 (1990) 1020–1055.